J. Appl. Comput. Mech., 10(1) (2024) 80-91
DOI: 10.22055/jacm.2023.43947.4148
ISSN: 2383-4536
jacm.scu.ac.ir

Shahid Chamran University of Ahvaz

Journal of Applied and Computational Mechanics

Research Paper

Optimizing Multidirectional Torsional Hysteretic Damper Specifications using Harmony Search

Arash Radman[1], Saeid Pourzeynali[2], Nima Faraji[3]

[1] Eastern Faculty of Engineering, University of Guilan, Guilan, Iran, Email: a.radman@guilan.ac.ir

[2] Department of Civil Engineering, Faculty of Engineering, University of Guilan, Guilan, Iran, Email: pourzeynali@guilan.ac.ir (S.P.); nimaafaraji76@gmail.com (N.F.)

Received June 01 2023; Revised September 06 2023; Accepted for publication September 21 2023.
Corresponding author: A. Radman (a.radman@guilan.ac.ir)

Abstract. Multidirectional torsional hysteretic damper is a new type of damper that can be used to isolate and dissipate seismic effects on a structure. It can be designed to have a controllable post-elastic stiffness and exhibit high levels of damping as well as stable cyclic response. In this article, while offering a simplified numerical relationship for force-displacement response of the damper, the structure that is fitted with this innovative type of damper is optimized using the harmony search optimization procedure with discrete design variables. Numerical experiments show that the harmony search methodology can determine the damper parameters with high computational efficiency and outperform genetic algorithm and simulated annealing procedure in this regard.

Keywords: Harmony Search, Structural optimization, Multidirectional torsional hysteretic damper, seismic isolation, Genetic Algorithm, Simulated Annealing.

1. Introduction

Researchers have looked into a number of cutting-edge techniques for making resilient buildings in addressing the long-standing concern about earthquake damages. There are several methods that are currently being researched to mitigate and better explore the effects of earthquake, including structural frames with rocking columns as an energy dissipating mechanism [1], new performance spectra-based methods [2] and application of self-centering damper with a shape memory alloy [3], to name a few. Among various methods, utilizing seismic isolators is one of the methods that reduces the impact of earthquakes on structures by increasing the period of the structure and bringing it into the low energy part of a design spectrum. However, the use of seismic isolators without dampers, might lead to substantial earthquake-induced deformations. Dampers dissipate a part of energy absorbed by the structure; in this way, the demand for displacement and ductility is reduced. At the same time, the addition of dampers can increase the stiffness and decrease the period of the structure, which counteracts the first mechanism (increasing the period owing to the use of isolators). Therefore, based on the behavior of a structure, it is necessary to use a suitable combination of isolators and dampers in the design.

Although the research on the application of seismic isolation systems goes back about 150 years [4], in the past 50 years, there has been a growing interest in using additional mechanisms, such as isolators and dampers, to control the structures' behavior during earthquake events, and numerous studies have been conducted on development and better understanding of the performance of such systems. Investigating the effects of different metals in friction dampers [5], using winding rope viscous dampers to reduce the effects of earthquakes on bridges [6], using new types of lead-viscoelastic coupling beam damper [7], application of hysteretic metal dampers [8], liquid dampers [9, 10] and memory alloys [11] are examples of ongoing research in the development of isolators and dampers.

The energy dissipation mechanism in metallic dampers is generally through entering the non-linear part of the material's response in some elements, and transforming it to heat in alternating cycles of displacement [12] or hysteretic behavior. One of the important considerations in the design of hysteretic dampers is the distribution of plastic strains. The uniformity of the strain, especially in the plastic state, can reduce the fatigue of material and causes the stability of the hysteretic curve. The uniformity of strain can also increase the deformation capacity of the member. When bending members are used in a hysteretic damper, the energy dissipation is usually concentrated in an area called the plastic hinge, and the displacement (rotation) capacity is relatively limited. On the other hand, in a cylinder under torsion, uniform stresses and strains are applied to all points that are at equal radial distances along the height of the section. Such a state of stress and strain occurs in both elastic and plastic phases of material response. This situation does not occur in non-cylindrical cross sections under torsion, in which some parts enter the plastic stage earlier. Concentration of plastic strains in the corners of a non-cylindrical section, reduces the fatigue resistance of the section under hysteretic loading [13].

Published online: September 29 2023

There have been studies on the use of metallic materials in torsion as hysteretic dampers, however displacement and energy dissipation frequently happened in a particular direction in these studies [13, 14]. A relatively new type of damper, known as "multi-directional torsional hysteretic damper" (MTHD) [15] is a mechanical device that is installed between two points of the structure where isolation and damping is intended. It is basically designed for seismic isolation of bridges, although it can be used for other structures. As a result of horizontal movements of the supporting points, energy-dissipating cylinders undergo various stages of torsional yielding or hardening. MTHD can be designed to have a controllable post-elastic stiffness and to exhibit high levels of damping as well as a stable hysteretic response. The kinematic function of MTHD is described in the next section in more details. Despite the mentioned advantages, limited applications have been reported, partly due to the complex relationship between force and displacement that exists in this type of damper.

On the other hand, to simplify the structural design procedures, numerous studies have employed optimization algorithms in various forms. There are several meta-heuristic algorithms that have been created, which vary in terms of effectiveness, computational cost, or the work needed to be adjusted for a particular calculation. [16]. These methods have been widely used for optimizing the response of structures against earthquakes. The use of shape optimization to improve U-shaped dampers [17], use of "simulated annealing algorithm" for optimization of "shear panel dampers" [18], use of "artificial bee colony algorithm" to determine the optimal location of viscous dampers in a structure [19], using "chaotic optimization algorithm" for optimization of "tuned mass damper" parameters [20], using "swarm intelligence" to simultaneous optimize viscous dampers and tuned mass damper [21] and application of magneto-rheological dampers using fuzzy logic [22] are among extensive research that have been done in this respect.

Harmony search is a meta-heuristic optimization algorithm that was proposed by Geem in 2000 [23], Harmony search imitates the music player's improvisation in trying to find a more balanced harmony, which is analogous to solving engineering design problems. It benefits from some of the features of the existing algorithm, such as using sets of design variables, but at the same time it allows for different adaptation rates which is in line with more advanced algorithm such as simulated annealing. To decrease the probability of trapping in local optima, harmony search works on a population of solutions simultaneously, which is similar to genetic algorithm; however, in contrary to genetic algorithm which uses only two existing sets of design variables for improving the solution, harmony search improves the solution using all feasible sets of design variables. Also, the efficiency of each solution is obtained directly from the system analysis, so there is no need for additional variables, such as the derivative of the objective function with respect to design variables (so-called sensitivity numbers). These properties make the methodology versatile, especially in solving complex functions of design variables. More details about the structure of the algorithms will be presented in section 3. In addition to its many applications in solving various engineering problems, the method has been used in many researches for designing base isolators and dampers such as in [24-26].

In this paper, in addition to presenting a simplified force-displacement relationship for finite element modelling the MTHD behavior, the harmony search methodology [27] is used to optimize its characteristics. In the following sections, the MTHD kinematics will be described and a simplified force-displacement relationship will be presented, which is necessary for finite element modelling and numerical time-history analyses. The details of harmony search algorithm will be presented and its efficiency in determining the damper parameters will be demonstrated through a numerical example and compared with known optimization algorithms.

2. Multidirectional Torsional Hysteretic Damper

2.1. Introduction

Figure 1 shows a general view and a section of the MTHD, which consists of two parts [28]. The upper part, (consisting the rails and upper steel plate), is connected to the superstructure and the lower part is fixed on the foundation or pedestal. The connection of the upper and lower parts is through a number of rails. The lower part includes a steel short-column at the center, which transfers bending moments to the foundation. There are eight solid steel cylinders around the short-column, which dissipate energy through yielding in torsion. The connection of the short-column to the bottom baseplate and the lower steel plate is fixed. But the eight energy- dissipating cylinders are connected to eight arms at the top, which in turn are engaged with the upper part by the rails. The arms are connected to the rails by sliding parts, which can rotate and move freely along the rail path and can be made with plastic or metal. Note that the rails do not rotate under any condition and are always parallel to the initial position of the arms. If friction is ignored, no axial force is developed in the arms with this type of connection. The connections are designed so as to allow the damper to move horizontally in any direction [28, 29].

The rails are welded to the upper steel plate, which is attached to the superstructure. It can be seen that the upper and lower parts of the damper are apart, which reduces the sensitivity of the device to vertical displacements. When the superstructure moves horizontally under the effect of a lateral force, the arms engaged with the rails transform the displacement to torsion in the eight energy dissipating cylinders as shown in Fig. 2. The torsion can cause the cylinders to enter a post-elastic phase. The short-column prevents the formation of bending moment in the cylinders; therefore, the energy dissipating cylinders are subject to relatively uniform yielding due to torsion [28, 29].

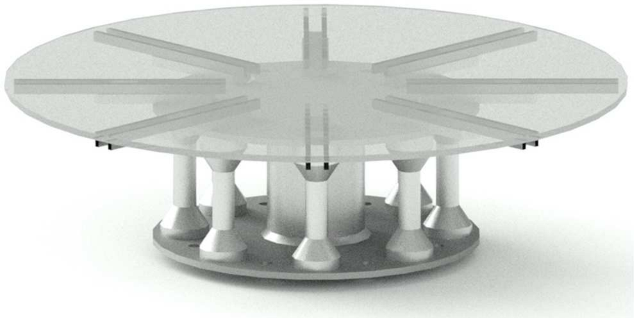

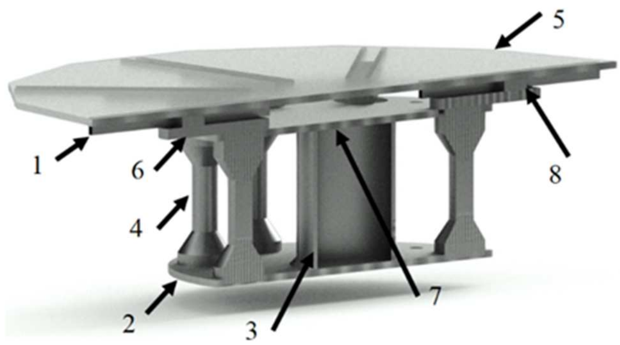

Fig. 1. General view and a section of MTHD. (1) Rail, (2) Base plate, (3) Short column, (4) Energy dissipating cylinders, (5) Upper steel plate, (6) Arm, (7) Lower steel plate, (8) Sliding parts.

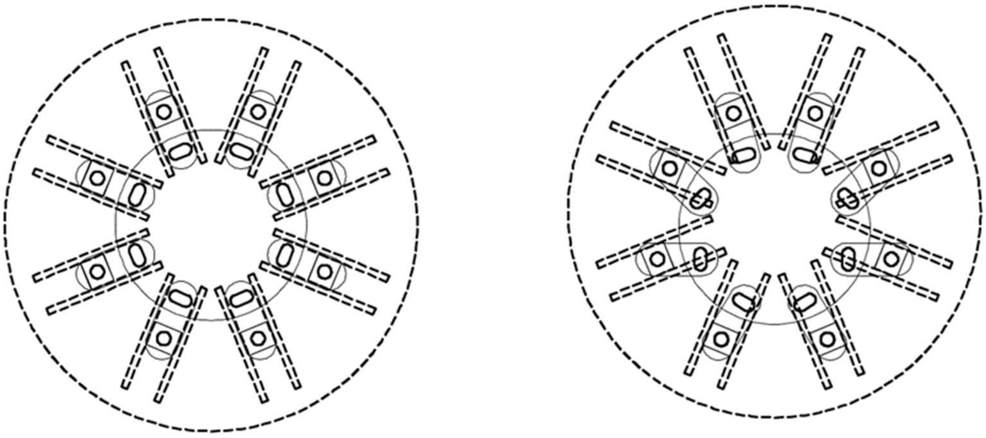

Fig. 2. Kinematic of MTHD. Left: initial position. Right: displaced position.

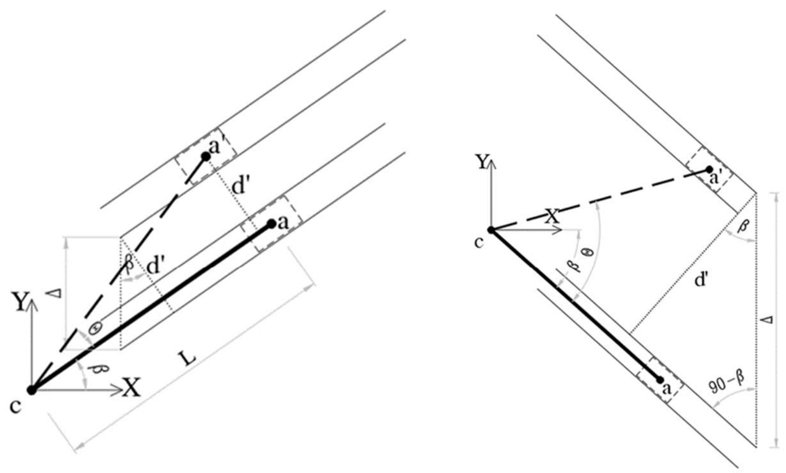

(a) $0 \leq \beta < 90^{\circ}$ (b) $-90^{\circ} < \beta \leq 0$

Fig. 3. Displacement-twist angle relationship in MTHD.

For time-history analysis and finite element modelling of a structure with MTHD, it is necessary to establish a displacement-force relationship for the damper; but as mentioned, this relationship is complex [15]. Dimensionless diagrams have been proposed by the device inventors [15], which present the displacement-force relationship based on a number of device characteristics. These features can include the maximum force that can be carried by the device, the maximum lateral displacement due to the above force and the yielding force. Alternatively, the maximum force that can be carried by the device, the maximum lateral displacement due to the above force and the hardening ratio can be used for predicting the response of the device [15]. However, these characteristics are dependent on the design parameters of the device a priori, such as the diameter and height of the energy dissipating cylinders, the length of the connected arms, and the ratio of device developed maximum force to yielding force (hardening ratio). For the finite element modelling and optimization of a building's behavior under time-history dynamic analysis, these characteristics may be defined as design variables; therefore, a numerical force-displacement relationship is required. The purpose of the next section is to provide a simplified relationship for calculating the displacement-force response, so that they can be used in an optimization-based analysis. The displacement-force relationship is obtained in 3 steps, as explained under sections 2.2 to 2.4.

2.2. Displacement-twist angle relationship

As mentioned, under the effect of movement of the upper part of the damper with respect to the lower part, the energy dissipating cylinders are subjected to different degrees of torsion (elastic or plastic) as shown in Fig. 2. In addition, there is some friction between moving parts, which in turn causes energy dissipation. The presence of friction makes the force-displacement response in the multidirectional torsional hysteretic damper complicated, but experimental verification tests show that the effects are negligible [15]; therefore, these effects are ignored to establish a simplified relationship here. Also, the presence of gaps between device components (which is related to manufacturing tolerances) affects the force-displacement response to a small extent, which is also ignored here. In the following, it is assumed that connecting arms are not aligned with the applied force.

Here, it is assumed that the movement takes place along Y direction (note that the results can be generalized to other situations). Figure 3(a) shows a situation where the initial angle of the arm, connecting to the dissipater, is greater than zero $\beta \geq 0$. As a result of the displacement Δ, the point a, at the end of the arm, moves to a' and the arm rotates by the angle θ. Considering the fact that the alignment of the rail does not change as a result of the movement, trigonometric relations give:

$$d' = \Delta \times \cos\beta \tag{1}$$

Since it is assumed that the axial stresses (due to friction) are negligible, the length of the arm does not change, hence:

$$\sin\theta = \frac{d'}{L} \tag{2}$$

From Eq. (1) and (2):

$$\theta = \sin^{-1}\left(\frac{\Delta \times \cos\beta}{L}\right) \tag{3}$$

It can be shown that Eq. (3) is valid for other initial positions of the arm, as shown in Fig. 3(b) for instance.

2.3. Twist angle-torsion relationship

One of the accepted theoretical relationships between stress and strain in mild steel is the Ramberg-Osgood model [30]. In this model, elastic ε_e and plastic ε_p strains are calculated from separate relationships and then added together to calculate the total strain. An exponential relationship is used for calculating the stress based on the plastic strain (the elastic strain is not included in the equation):

$$\sigma = H\varepsilon_p^n$$

The constants of the above equation are related to the characteristics of the steel and can be obtained from a logarithmic stress versus strain curve fitting; *n* is the "strain hardening exponent"; in the case which the curve is replaced by two asymptotes with equal logarithmic decay, *n* is the slope of the asymptote. The constant *H* is equal to the stress at unit plastic strain. *n* and *H* can be measured for different steels. The total strain is also obtained from the following relationship:

$$\varepsilon = \varepsilon_e + \varepsilon_p = \frac{\sigma}{E} + \left(\frac{\sigma}{H}\right)^{1/n} \tag{4}$$

The above relationship represents a continuous curve for stress and strain that does not have a definite yield point. However, it is possible to define a yield stress assuming ε_p = 0.002; in other words [30]:

$$\sigma_y = H \times 0.002^n \tag{5}$$

When a shaft is under torsion up to the yielding shear stress, the relationship between torsion, shear stress and shaft twist angle is expressed by the following equations:

$$T = \frac{\theta GJ}{H_l} \tag{6}$$

$$\tau = \frac{Gr\theta}{H_l} \tag{7}$$

where, H_l is the length of the shaft, *r* is the distance of the desired point for calculating the stress to the center of the shaft, and *J* is the polar moment of inertia of the shaft section. In a circular cylinder under torsion, all points are under pure shear stresses. If the z axis aligns with the shaft axis, the only non-zero stress component is τ_{xy}. In such a situation, the principal stresses and strains are as follows:

$$\sigma_1 = -\sigma_2 = \tau_{xy} \qquad ;\sigma_3 = 0 \tag{8}$$

$$\varepsilon_1 = -\varepsilon_2 = \frac{\gamma_{xy}}{2} \qquad ;\varepsilon_3 = 0 \tag{9}$$

When an element of a section enters the plastic region, the total strain in the principal directions is the sum of the elastic and plastic strains. For example, along the principal direction 1, it can be written:

$$\varepsilon_1 = \varepsilon_{e1} + \varepsilon_{p1} \tag{10}$$

where

$$\varepsilon_{e1} = \frac{1}{E}\left[\sigma_1 - \nu\left(\sigma_2 + \sigma_3\right)\right] = \frac{(1+\nu)}{E}\sigma_1 \tag{11}$$

The relationship between plastic strain and stress is expressed by a relationship similar to Hooke's law, with the difference being that Poisson's ratio of 0.5 is used. This value of Poisson's ratio is equivalent to assuming that the material does not undergo volumetric change during plastic strains. In such a case, it can be shown that the total strain in direction 1 is [30]:

$$\varepsilon_1 = \frac{(1+\nu)}{E}\sigma_1 + \frac{3}{2\bar{\sigma}}\sigma_1\left(\left(\frac{\bar{\sigma}}{H}\right)^{1/n}\right) \tag{12}$$

in which $\bar{\sigma}$ is the effective stress at which the yielding occurs and can be calculated using von Mises yield criterion. By the Eq. (5) and (9):

$$\gamma_{xy} = \frac{\tau_{xy}}{G} + \left(\frac{\tau_{xy}}{H_\tau}\right)^{1/n} \tag{13}$$

in which

$$H_\tau = \frac{H}{3^{(n+1)/2}} \tag{14}$$

It can be shown that with a Ramberg-Osgood material model, the relationship between the maximum shear stress and the torsion for a cylinder is [30]:

$$T = 2\pi R^3 \tau_R \left(\frac{0.25 + \frac{2n+1}{3n+1}\beta_\tau + \frac{n+2}{2n+2}\beta_\tau^2 + \frac{1}{n+3}\beta_\tau^3}{(1+\beta_\tau)^3} \right) \tag{15}$$

where τ_R is the shear stress at a point of the cross section farthest away from the center, and:

$$\beta_\tau = \frac{\gamma_{pR}}{\gamma_{eR}}$$

$$\gamma_{pR} = \left(\frac{\tau_R}{H_\tau}\right)^{1/n} \tag{16}$$

$$\gamma_{eR} = \frac{\tau_R}{G}$$

$$\gamma_R = \gamma_{eR} + \gamma_{pR}$$

2.4. Torsion-force relationship

The torsion-force relationship can be obtained by considering the geometry of the damper. Figure 4 shows two different situations of the damper arm. The goal is to obtain an expression for the force *F* component along the Y direction, (F_y). As a result of the rotation, the point (a) moves to the point (a'). Ignoring the friction, the resultant contact force between the sliding part and the rail (*F*) is perpendicular to the rail. The force *F* is divided into two components F_1 and F_2, perpendicular and parallel to the arm respectively. Due to the fact that the rail does not rotate, the following equations are valid for both cases shown in Fig. 4:

$$F_1 = F\cos\theta \tag{17}$$

$$L \times F_1 = T \tag{18}$$

$$F_y = F\cos\beta = \frac{T\cos\beta}{L\cos\theta} \tag{19}$$

Eq. (19) indicates that as the arm rotates, the required force for rotating changes. This type of geometric hardening or softening is one of the special features of MTHD and can be controlled by making geometric changes in the damper [10], in such a way that the overall response of the structure is optimized.

2.5. Cyclic loading and unloading

One of the common attributes of steel and some other metals is that after the first yielding has occurred, yielding occurs again when the stress difference reaches $2f_y$ in the unloading path. The slope of the unloading path is similar to the loading segment. Yielding in unloading occurs at a lower stress, which is also known as the Bauschinger effect. When the experimental data of loading and unloading are available, the following rules can be used to generate a stress and strain curve (or force-displacement) for cyclic loading [30]. Experimental verification tests also show the validity of these assumptions in prediction the MTHD behavior [28, 29]:

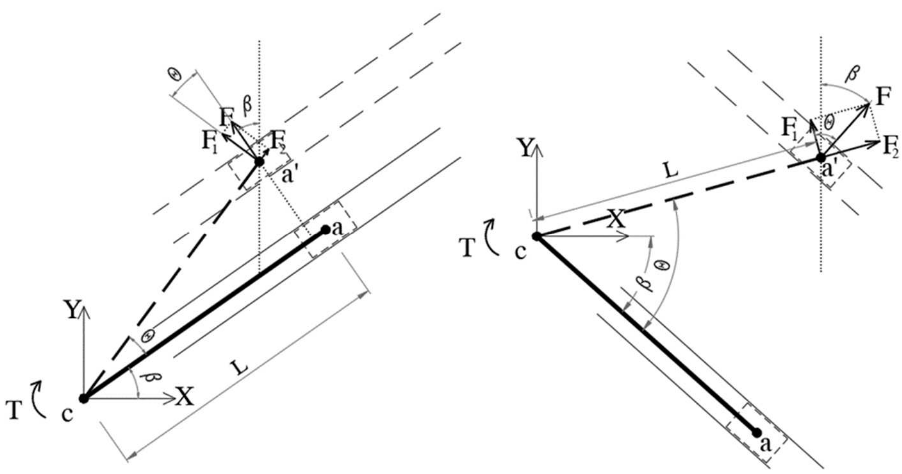

Fig. 4. Force-twist angle relationship of MTHD.

1: After the reversal of displacement direction, the slope of the force-displacement curve (between any two consecutive points of the diagram in the loading path) is repeated, in order, in unloading and the rest of loading and unloading sequences;

2: In the first unloading and the rest of cyclic loading sequences, the length of each segment of the graph is twice its value in the first loading;

3: An exception to the above rules is when a part of the loading segment is not used in unloading. In this case, this segment shall be skipped. (This case might occur when the displacement in unloading does not reach the ultimate displacement in initial loading and is asymmetric with respect to the origin).

2.6. Step-by-step procedure for obtaining force-displacement relationship

To summarize, the force-displacement relationship in the multidirectional torsional hysteretic damper can be obtained as follows:

Step 1: It is assumed that the height, diameter and length of the connecting arms of the energy dissipating cylinders are defined. The maximum displacement of the device is also a prescribed value (alternatively, the ratio of the maximum force in damper to the yielding force (HI) can be a defined value).

Step 2: Assume a value for displacement Δ.

Step 3: For each energy dissipating cylinder:

Step 3-1: Use Eq. (3) to obtain the rotation angle θ;

Step 3-2: Using Eq. (8) and (15), calculate the equivalent torsion developed in each energy dissipating cylinder;

Step 3-3: The force (along the direction of Δ), which is in equilibrium with the torsion of the previous step, is calculated using Eq. (19);

Step 4: Add the 8 energy dissipating cylinder forces obtained in step 3 together. This force along with the Δ in the step 2 will be a point in the force-displacement diagram;

Step 5: Increase the value of Δ and go to step 2;

Step 6: The diagram can be replaced with a bi-linear behavior. Note that in this case, the rate of hardening will affect the response of the structure even at small post-elastic deformations of the damper. Also, the diagram can be generalized for cyclic loading, using section 2.5.

The above steps can be programmed with a low computational cost.

2.7. Numerical example

In this example, the result of simplified procedure of section 2.6 has been compared with the results in reference [28]. It is assumed that the force-displacement relation is desired for a multi-directional torsional hysteretic damper, in which eight energy dissipating cylinders with angles of ± 67.5° and ± 22.5° are placed symmetrically with respect to the Y axis. The cylinders have a radius of 50 mm, a height of 411 mm, and the length of the arms is 558 mm. The steel is of S355J2 type, with a yield stress of f_y=470MPa. Through the analysis of the stress and strain diagram of the used steel, the Ramberg-Osgood model parameters are H=700MPa and n=0.047. The maximum force to the yielding force ratio of HI=2.2 is assumed for the damper. As an application of Eq. (6), the yielding force of F_y=698kN is calculated.

Figure 5 compares and shows a good agreement between the results from the above simplified procedure and the results in reference [28].

3. Harmony Search

Harmony search is a simple yet efficient, meta-heuristic algorithm that can be used to search for optimal values of either continuous or discrete design variables [31]. After doing a system analysis, a stochastic search technique is used in an iterative process, thus the objective function's derivatives with respect to the design variables are essentially unnecessary. To illustrate the method, assume that the optimization objective is to maximize the function $f(\mathbf{x})$, which $\mathbf{x}$ is a set of design variables (a design variable can be size, thickness, stiffness, and similar properties of a structure). Harmony search uses a matrix called "harmony memory" (**HM**). Each row of **HM** contains a set of design variables which defines a possible solution. The **HM** rows are sorted based on the performance of each set on the optimality of the objective function. The total number of **HM** rows is called "Harmony Memory Size" (*HMS*), and represents the number of solutions stored in **HM**. *HMS* is defined as an initial parameter empirically:

$$\mathbf{HM} = \begin{bmatrix} x_1^1 & x_2^1 & \cdots & x_j^1 \\ x_1^2 & x_2^2 & & x_j^2 \\ & \vdots & \ddots & \vdots \\ x_1^{HMS} & x_2^{HMS} & \cdots & x_j^{HMS} \end{bmatrix} \tag{20}$$

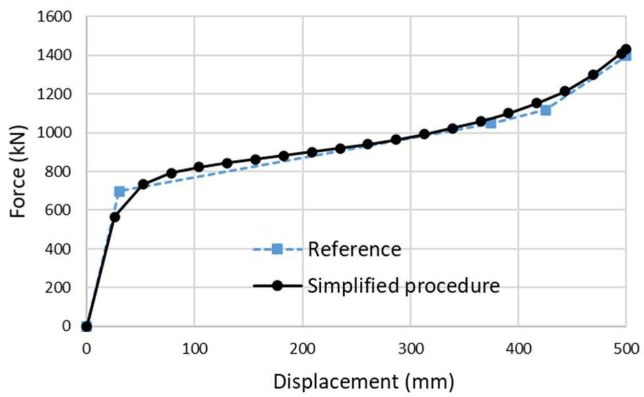

Fig. 5. MTHD force-displacement comparison between [28] and the simplified procedure.

At the beginning of the procedure, the elements of **HM** are selected from the entire possible range of design variables randomly. For each later iteration, a new set of design variables is selected as described below, the system is analyzed and the performance of selected design variables is measured. If the selected set has a better performance on improving the objective function, the new set is replaced with the worst set in **HM**. The procedure continues until the maximum iteration number or time is reached or the objective function cannot be improved [23].

New set of design variables can be selected randomly, either from the possible range or from the values already stored in **HM**. This is implemented through three stochastic procedures called "memory considerations", "pitch adjustments" and "randomization".

The "memory considerations" uses an empirical value called "harmony memory consideration rate" (*HMCR*), which is usually a real number between 0 and 1, and is defined as an initial, usually constant, parameter of the algorithm. *HMCR* is the probability of selecting the design variable from one of its previous values in **HM**. For this purpose, a random and real number (between 0 and 1) is assigned to each design variable (*randi*) at the beginning of each iteration. If *randi* < *HMCR*, the next value of the design variable will be randomly selected from one of its values in **HM** through the "pitch adjustments" procedure. Otherwise, the next design variable is selected by the "randomization" procedure.

The "pitch adjustment" procedure uses another empirical parameter called the "pitch adjustment rate" (*PAR*). *PAR* is an initial parameter of the algorithm and is determined by numerical experiments. In the basic form of harmony search, *PAR* is usually a constant and real number between 0.3 and 0.4. It allows for permutation of the design variables when they are supposed to be selected randomly from values in **HM**. When the algorithm is formulated with discrete design variables, *PAR* defines the probability of changing a randomly selected design variable from a row of **HM** with an upper or lower row value.

If the random number assigned to a design variable, *randi* > *HMRC*, the next design variable is randomly selected from the entire range of possible values, which is called "randomization" procedure in this context.

4. Methodology

4.1. Problem statement

For the design of a structure against dynamic loads, features such as relative floor drifts, speed, acceleration, absorbed energy, etc. can be considered as the objective of optimization (objective function). The behavior of a structure equipped with a damper depends on the physical characteristics of the damper. As mentioned in the previous sections, the response characteristics of a multi-directional torsional hysteretic damper depend on attributes such as the height (H_l), diameter (D), the length of the arms connected to the energy dissipating cylinders (L) and the degree of hardening of the damper (Hl). If the objective is to limit the floor drifts to a prescribed value under nonlinear time-history analysis, the optimization problem can be expressed in the following form:

$$\begin{gathered}\text{Minimize}: f(x)=\sum_{1}^{n}\left|d_i-d_i^{*}\right| \\ \text{Subject to: } \mathbf{m}\ddot{\mathbf{u}}+\mathbf{c}\dot{\mathbf{u}}+\mathbf{k}\mathbf{u}=-\mathbf{m}\ddot{\mathbf{u}}_{\mathrm{g}}(t)\end{gathered} \tag{21}$$

where d_i is the maximum drift of the floor i; n is the total number of floors in the structure, d_i^{*} is the prescribed floor drift; **m**, **c** and **k**, are mass, damping and stiffness matrices of the structure respectively; **u** is the time dependent displacement vector and $\ddot{\mathbf{u}}_{\mathrm{g}}$ is the ground acceleration.

4.2. Algorithm

Based on the basic harmony search algorithm, a solution for determining the specifications of the multidirectional torsional hysteretic damper in order to optimize the response of the structure can be defined in the following steps:

1. Determine the objective function and parameters of the harmony search algorithm such as *HMS*, *HMCR*, *PAR*;
2. Determine the acceptable range of quantities for damper specifications such as the diameter and height of energy dissipating cylinders, arm length and hardening ratio (D, H_l, L and Hl, respectively);
3. Considering D, H_l, L and Hl as design variables, *HMS* sets of design variables are randomly selected from the entire range. For each set, MTHD force-displacement relationship is established, and the response of the system is calculated. The sets are sorted according to their effect on the objective function and stored in **HM**;
4. With the help of three procedures of "memory considerations", "pitch adjustment" and "randomization" a new set of design variables is selected;
5. The force-displacement curve and the system response are calculated;
6. If the response of the system is better than one of the sets stored in **HM**, the new set is replaced with the worst set;
7. Steps 4 to 6 are repeated until the objective function cannot be improved or the maximum number of iterations has been reached.

5. Numerical Experiments and Discussion

5.1. Example 1

To verify the effectiveness of the described method, the objective of this example is to find the optimized damper specifications for a structure with minimized drifts, so that the displacement of the damper does not exceed 80% of the device allowed value:

$$\text{Minimize} \quad f(x)=\sum_{1}^{n}\left(d_i-d_i^{*}\right)^2 \tag{22}$$

$$\text{Subject to}: \left|u_{damper}\right| \le 0.8\times u_{max} \tag{23}$$

and

$$\mathbf{m}\ddot{\mathbf{u}}+\mathbf{c}\dot{\mathbf{u}}+\mathbf{k}\mathbf{u}=-\mathbf{m}\ddot{\mathbf{u}}_{\mathrm{g}}(t) \tag{24}$$

in which u_{damper} represents the maximum displacement of the damper and u_{max} is its maximum allowed. Other parameters have been defined under Eq. (21).

For imposing the condition of Eq. (23), any randomly generated solution with $|u_{damper}| > 0.8 \times u_{max}$ may not be allowed in **HM**; However, here Eq. (22) and (23) are combined together using a penalty scheme in the form of Eq. (25), to better explore the solution near the limits in this example:

$$\text{Minimize}: \sum_{1}^{n}\left(d_i - d_i^*\right)^2 \times \left(\left|\left|u_{damper}\right| - 0.8\times u_{max}\right|\right)^p$$
$$\text{Subject to: } \mathbf{m\ddot{u}} + \mathbf{c\dot{u}} + \mathbf{ku} = -\mathbf{m\ddot{u}_g}(t) \tag{25}$$

in which p is a penalty exponent, chosen experimentally (p = 2 for this example).

A 4-story framed structure has been subjected to a scaled Imperial Valley earthquake of October 15, 1979. The lumped masses at story levels are 103.6 tons. The stiffnesses are 12000, 7500, 5000 and 2500 N/mm from the bottom story to the top, respectively. The structure, including 4 dampers which are defined at the base, was modeled with 5 translational degrees of freedom. All stories remain within elastic range except for the dampers which may demonstrate a non-linear behavior. The Rayleigh damping model is considered with a damping ratio of 3 percent. The prescribed drifts are d_i^* = 0.002 for all stories in this example.

The problem has 4 design variables, including the diameter of the energy dissipating cylinders D, the length of the arms connecting the cylinders L, the height of the cylinders H_l and the ratio of maximum tolerable force to yielding force HI. The design variable D ranges from 15 mm to 70 mm in 23 different sizes, the parameter H_l can be selected from 150 mm to 350 mm in 41 sizes, the design variable L is from 220 mm to 700 mm in 77 different sizes, and the HI varies from 1.4 to 2.3 with 0.1 increments; therefore, the total possible permutations of variables are 726110.

The size of the harmony memory matrix **HM** is HMS=5; in addition, $HMCR$=0.75 and PAR=0.3 are selected for this example.

Figure 6 shows the variations of the best answer, stored in **HM** throughout the optimization procedure. For the harmony search method, the optimization time for 315 iterations is 1000 seconds in a core i7 CPU and it takes 300 iterations to arrive at the objective function value of 0.1 as per Eq. (25). The obtained parameters are D=32mm, H_l=225mm, L=440mm and HI=1.9.

Figure 7 shows the dampers displacement time-history for the best answer obtained with harmony search. The maximum displacement is 310mm which is approximately 80% of the maximum allowed (387mm). Figure 8 shows the time-history of stories' drifts for the best answer.

Figure 6 also compares the results of a harmony search run with a generational genetic algorithm and simulated annealing optimization procedures. For the genetic algorithm, a generalized method (offspring replace their parents) [32] has been used, in which, a population size of 5, elitism factor of 0.5, mutation rate of 0.2 and mutation probability of 0.5 have been applied. For the simulated annealing procedure [33] an exponential temperature update function together with Boltzmann annealing function have been selected.

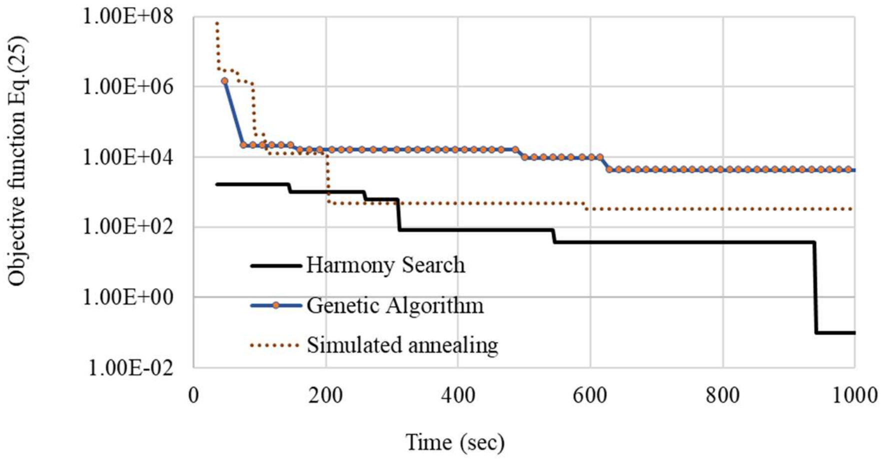

Fig. 6. Variations of the best solution vs. time.

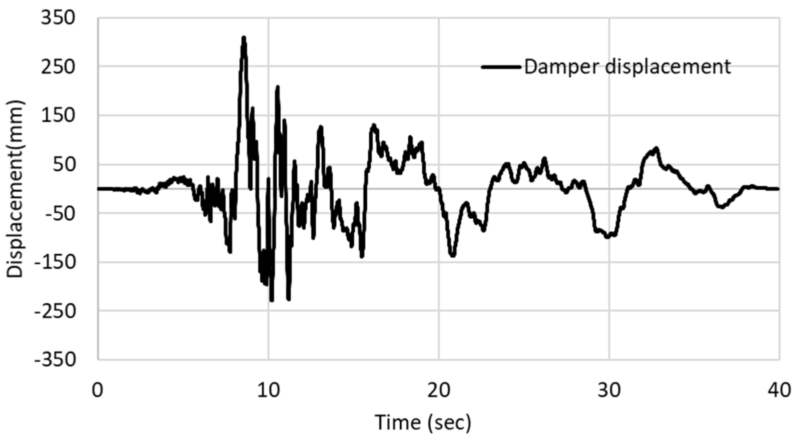

Fig. 7. Time-history of damper displacement for the best solution.

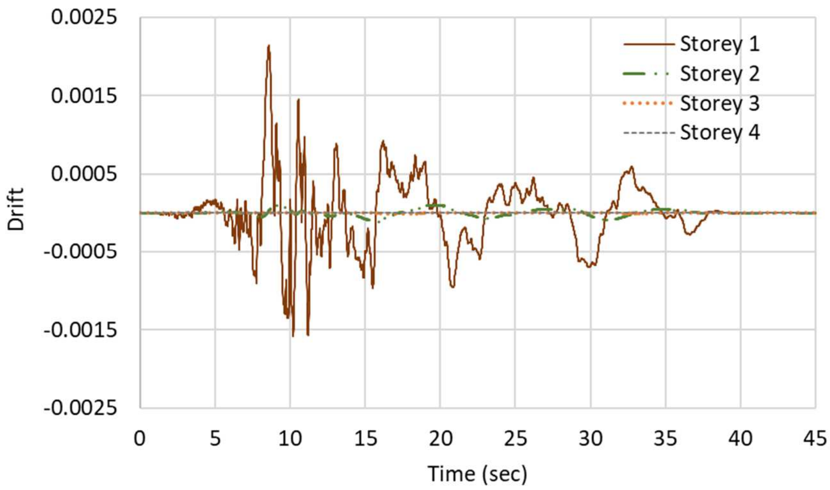

Fig. 8. Time-history of stories' drifts for the best solution.

To better compare the computational efficiency of the applied harmony search algorithm with genetic algorithm and simulated annealing optimization procedures, one-tailed tests have been performed. Each procedure was run 30 times for 1000 seconds and the average and variance of the resulting objective function have been computed as shown in Table 1 and Table 2. As it can be seen, the average value of the objective function is smaller for harmony search in both cases, for this minimization problem. The tables also show the one-tailed test p values which are less than the significance level (0.1), rejecting the null hypothesis that the two methods have similar performance in each case.

The computational efficiency of harmony search has been compared with that of genetic algorithm through a number of studies [34-37]. The consensus is that harmony search outperforms, which is attributed to lesser dependence on the selection of algorithm parameters [35].

5.2. Example 2

To illustrate the effect of MTHD in reducing the excitation of buildings, a 2D frame of 8-story building with total height of 32m and 6×6m bays with a total width of 36m, has been used in this example. With the frame tributary width of 5m, the dead and live loads of the building are 7 and 2 kN/m^2 on each story, and 6 and 2 kN/m^2 on the roof respectively. The preliminary sections selected for the analysis are columns of HE400B for the stories 1 to 4, HE300A for the stories 5 and 6 and IPE300 for the stories 7 and 8. The beam sections are IPE400 for the stories 1 to 4, IPE360 for the stories 5 and 6 and IPE300 for the stories 7 and 8. All profiles conform with St-52 steel properties.

Table 1. Comparison between genetic algorithm and harmony search through one-tailed test for 1000sec runtime.

	Genetic Algorithm	Harmony Search
Run numbers	30	30
Average value of Equation (25)	178.372	40.159
Variance	157264.302	7278.066
One t-test p value	0.0336	

Table 2. Comparison between simulated annealing algorithm and harmony search through one-tailed test for 1000sec runtime.

	Simulated Annealing	Harmony Search
Run numbers	30	30
Average value of Equation (25)	253.283	40.159
Variance	590609.886	7278.066
One t-test p value	0.0708	

Table 3. Selected records and optimized damper parameters.

Analysis No.	NGA-West 2 database RSN	Event	Date/ Station/ Azimuth	Optimized MTHD properties			
				D (mm)	*H_l (mm)*	*L (mm)*	*HI*
TH-1	4481	L'Aquila Italy	4/6/2009, L'Aquila - V. Aterno -Colle Grilli, N	30	215	275	2.3
TH-2	4482	L'Aquila Italy	4/6/2009, L'Aquila - V. Aterno -F. Aterno, N	34	150	220	1.9
TH-3	5618	Iwate	6/13/2008, IWT010, EW	24	225	305	1.9
TH-4	285	Irpinia Italy-01	11/23/1980, Bagnoli Irpinio, 270˚	42	150	230	2
TH-5	4864	Chuetsu-oki	7/16/2007, Yoitamachi Yoita Nagaoka, EW	28	170	245	1.9
TH-6	4854	Chuetsu-oki	7/16/2007, Nadachiku Joetsu City, EW	26	155	290	1.9
TH-7	4858	Chuetsu-oki	7/16/2007, Tokamachi Chitosecho, EW	24	175	290	2.3
TH-8	5806	Iwate	6/13/2008, Yuzawa Town, NS	25	175	255	1.9
TH-9	2626	Chi-Chi Taiwan-03	9/20/1999, TCU075, E	28	160	220	1.9
TH-10	2734	Chi-Chi Taiwan-04	9/20/1999, CHY074, N	38	155	290	1.9
TH-11	801	Loma Prieta	10/18/1989, San Jose - Santa Teresa Hills, 225˚	25	230	235	1.9
TH-12	125	Friuli Italy-01	5/6/1976, Tolmezzo, N	38	280	250	1.9

Table 4. Reduction in drifts and base shear as a result of using MTHD wrt fixed base structure (minus sign indicates an increase).

Analysis No.	Story Drift (%)								Base Shear (%)
	0-1	1-2	2-3	3-4	4-5	5-6	6-7	7-8	
TH-1	12.2	38.3	35.4	28.1	22.1	24.9	26.0	33.4	77.4
TH-2	12.8	33.8	35.3	28.0	20.5	34.0	37.5	31.5	81.9
TH-3	9.2	32.1	30.2	26.6	31.9	40.8	41.6	34.3	80.2
TH-4	-12.1	16.2	0.7	8.1	16.6	19.6	32.6	30.4	75.9
TH-5	-30.9	6.3	15.4	17.7	22.5	29.6	27.2	42.3	72.5
TH-6	-5.2	21.3	23.4	22.0	19.9	17.7	18.1	35.8	77.9
TH-7	-12.6	12.2	15.2	21.3	21.3	27.8	44.9	51.2	78.8
TH-8	-28.0	7.0	17.2	24.9	29.0	36.3	38.3	39.3	75.0
TH-9	8.6	27.6	30.3	33.7	25.3	13.0	30.0	41.1	80.8
TH-10	5.2	23.5	24.7	16.7	20.1	25.7	22.2	22.3	80.9
TH-11	5.2	23.5	24.7	16.7	20.1	25.7	22.2	22.3	80.9
TH-12	-6.9	21.6	22.1	18.4	12.9	29.5	38.6	37.9	79.1

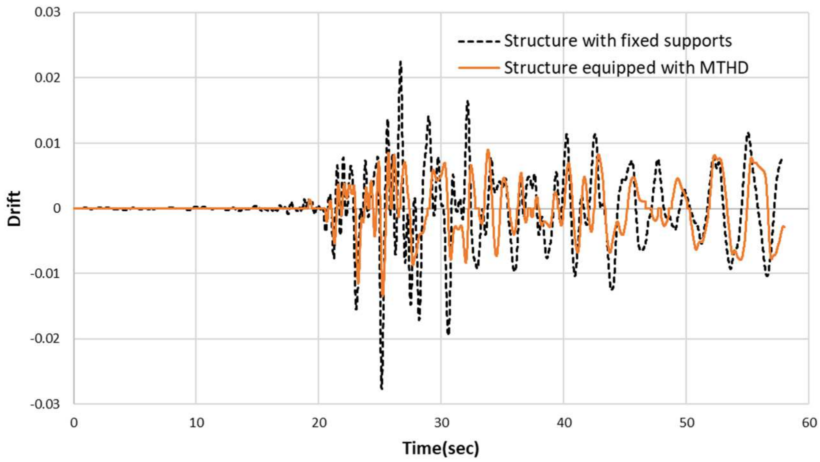

Fig. 9. Time-history of drift under TH-7 record in the 8th story.

The building locates in a site class C as per ASCE 7-10 definition, with spectral acceleration S_s=1.304 and one second spectral acceleration S_1=0.553. The response modification factor of 4.5 for an intermediate steel moment resisting frame and the occupancy importance factor of I_e=1.25 have been assigned for this building. Twelve acceleration-time series have been selected from NGA-West 2 database with magnitude ranging 5.5 to 7.5 and epicentral distance of maximum 100 km, which are appropriate for the building conditions. Table 3, presents the selected records information, which further scaled to match with the ASCE 7-10 design spectrum.

The objective function of Eq. (25), has been used for this example with a prescribed drift of d_i^*=0.002 for all stories. The harmony search parameters are HMS=5, $HMCR$=0.75 and PAR=0.3. The design variables of dampers (one at each column base), such as the diameter of the energy dissipating cylinders D, the length of the arms L, the height of the cylinders H_l and the ratio of maximum tolerable force to yielding force HI have similar ranges to the previous example. For each earthquake record the harmony search algorithm was run for 120 iterations, and the optimized MTHD parameters are evaluated as shown in Table 3.

The table shows that the MTHD optimal design parameters are very erratic in nonlinear time history analyses for different earthquakes, which emphasizes the necessity of using an optimization algorithm for methodical parameter determination.

Based on the results of Table 3, the average design parameters of D=30mm, H_l=185mm, L=260mm and HI=2.0 have been selected for the building. To compare the effects of using MTHD, the structure has been analyzed twice, once with assuming fixed supports at the columns bases and once assuming MTHD (with the averaged parameters) at each column base. The effects of MTHD in the base shear demand and drifts have been shown in Table 4. Figure 9 compares the drift at the top story under earthquake record TH-7 as an example. As it can be seen the MTHD reduces the demand on the building significantly.

6. Conclusion

In this study, the harmony search optimization methodology was used to determine the optimum properties of a new type of damper, namely, the multidirectional torsional hysteretic damper. A simplified force-displacement procedure has been presented for the calculation of the response of this type of damper, which is useful for numerical time-history analysis of the structures under earthquake loading and optimization of the structural performance. Numerical experiments show that the applied harmony search optimization algorithm can determine the damper parameters with a high computational efficiency under non-linear time-history analyses. The results show that the harmony search, that is tailored for discrete design variable optimization, outperforms that of genetic algorithm and simulated annealing optimization methods in determining the damper properties.

Author Contributions

A. Radman was involved in conceptualization, development of methodology, development of software, formal analysis, investigation, writing original draft, writing the final draft, visualization and project administration. S. Pourzeynali was involved in validation, review, editing and supervision. N. Faraji was involved in data curation and software development. All authors discussed the results, reviewed, and approved the final version of the manuscript.

Acknowledgments

This research did not receive any specific grant from funding agencies in the public, commercial, or not-for-profit sectors.

Conflict of Interest

There is no competing interest.

Funding

The authors received no financial support for the research, authorship, and publication of this article.

Data Availability Statements

The datasets generated and/or analyzed during the current study are available from the corresponding author on reasonable request.

References

[1] Zhang, P., Yam, M.C.H., Ke, K., Zhou, X., Chen, Y., Steel moment resisting frames with energy-dissipation rocking columns under near-fault earthquakes: Probabilistic performance-based-plastic-design for the ultimate stage, *Journal of Building Engineering*, 54, 2022, 104625.
[2] Ke, K., Zhou, X., Zhu, M., Yam, M.C.H., Wang, Y., Zhang, H., Seismic evaluation of industrial steel moment resisting frames with shape memory alloys using performance-spectra-based method, *Journal of Building Engineering*,48, 2022, 103950.
[3] Ke, K., Yam, M.C.H., Zhang, P., Shi, Y., Li, Y., Liu, S., Self-centring damper with multi-energy-dissipation mechanisms: Insights and structural seismic demand perspective, *Journal of Constructional Steel Research*, 204, 2023, 107837.
[4] Touaillon, J., *USA Patent No. 99973A*, 1870.
[5] Gao, J., Wang, C.-L., Meng, S., Zeng, B., Performance evaluation of friction dampers considering different metal pairs and loading rates, *Journal of Constructional Steel Research*, 204, 2023, 107859.
[6] Su, L., Zhang, W., Yang, T.Y., Chen, Y., Numerical and experimental investigations on the seismic response of continuous girder bridge using winding rope fluid viscous dampers, *Soil Dynamics and Earthquake Engineering*, 168, 2023, 107818.
[7] Fang, X., Zhou, Y., Bi, K., Hao, H., Wang, T., Experimental study on the cyclic behaviors of an innovative lead-viscoelastic coupling beam damper (LVCBD), *Journal of Building Engineering*, 64, 2023, 105596.
[8] Javidan, M.M., Ali, A., Kim, J., A steel hysteretic damper for seismic design and retrofit of precast portal frames, *Journal of Building Engineering*, 57, 2022, 104958.
[9] Aliev, F.A., Aliev, N.A., Velieva, N.I., Safarova, N.A., Larin Parameterization to Solve the Problem of Analytical Construction of the Optimal Regulator of Oscillatory Systems with Liquid Dampers, *Journal of Applied and Computational Mechanics*, 6, 2020, 1426-1430.
[10] Dezvareh, R., Upgrading the Seismic Capacity of Pile-Supported Wharfs Using Semi-Active Liquid Column Gas Damper, *Journal of Applied and Computational Mechanics*, 6(1), 2020, 112-124.
[11] Qiu, C., Jiang, T., Peng, L., Liu, J., Du, X., Seismic performance evaluation and design of resilient knee braced frames equipped with shape memory alloy knee braces and replaceable energy-dissipating connections, *Engineering Structures*, 283, 2023, 115918.
[12] Christopoulos, C., Filiatrault, A., *Principles of Passive Supplemental Damping and Seismic*, Pavia, Italy: IUSS 2006.
[13] Dusi, A., Bettinali, F., Forni, M., La Grotteria, M., Castellano, M., Infanti, S., . . ., Bonacina, G., Implementation and validation of finite element models of steel hysteretic torsional energy dissipators, *in 12th World Conference on Earthquake Engineering*, 2000.
[14] Skinner, R.I., Kelly, J.M., Heine, A.J., Hysteretic dampers for earthquake-resistant structures, *Earthquake Engineering & Structural Dynamics*, 3(3), 1974, 287-296.
[15] Dicleli, M., Milani, A.S., MARTI and MRSD: Newly Developed Isolation-Damping Devices with Adaptive Hardening for Seismic Protection of Structures, *World Academy of Science, Engineering and Technology, International Journal of Civil, Environmental, Structural, Construction and Architectural Engineering*, 9, 2015, 702-706.
[16] Halim, A.H., Ismail, I., Das, S., Performance assessment of the metaheuristic optimization algorithms: an exhaustive review, *Artificial Intelligence Review*, 54(3), 2021, 2323-2409.
[17] Deng, K., Pan, P., Su, Y., Xue, Y., Shape optimization of U-shaped damper for improving its bi-directional performance under cyclic loading, *Engineering Structures*, 93, 2015, 27-35.
[18] Deng, K., Pan, P., Sun, J., Liu, J., Xue, Y., Shape optimization design of steel shear panel dampers, *Journal of Constructional Steel Research*, 99, 2014, 187-193.
[19] Sonmez, M., Aydin, E., Karabork, T., Using an artificial bee colony algorithm for the optimal placement of viscous dampers in planar building frames, *Structural and Multidisciplinary Optimization*, 48, 2013, 395-409.
[20] Kaveh, A., Javadi, S.M., Mahdipour Moghanni, R., Optimal structural control of tall buildings using tuned mass dampers via chaotic optimization algorithm, *Structures*, 28, 2020, 2704-2713.
[21] Pourzangbar, A., Vaezi, M., Optimal design of brace-viscous damper and pendulum tuned mass damper using Particle Swarm Optimization, *Applied Ocean Research*, 112, 2021, 102706.
[22] Pourzeynali, S., Bahar, A., Pourzeynali, S., Semi-active control of vertical vibration of suspension bridges subjected to earthquake excitations using MR dampers and fuzzy logic, *Sharif Civil Engineering*, 322, 2016, 43-54.
[23] Geem, Z.W., Kim, J.H., Loganathan, G.V., A New Heuristic Optimization Algorithm: Harmony Search, *Simulation*, 76(2), 2001, 60-68.
[24] Nigdeli, S.M., Bekdas, G., Alhan, C., Optimization of seismic isolation systems via harmony search, *Engineering Optimization*, 46(11), 2014, 1553-1569.
[25] Ocak, A., Melih Nigdeli, S., Bekdas, G., Optimization of the base isolator systems by considering the soil-structure interaction via metaheuristic algorithms, *Structures*, 56, 2023, 104886.
[26] Bekdas, G., Nigdeli, S.M., Estimating optimum parameters of tuned mass dampers using harmony search, *Engineering Structures*, 33(9), 2011, 2716-2723.
[27] Zhang, T., Geem, Z.W., Review of harmony search with respect to algorithm structure, *Swarm and Evolutionary Computation*, 48, 2019, 31-43.
[28] Salem Milani, A., Dicleli, M., Systematic development of a new hysteretic damper based on torsional yielding: part I—design and development, *Earthquake Engineering & Structural Dynamics*, 45(6), 2016, 845-867.
[29] Salem Milani, A., Dicleli, M., Systematic development of a new hysteretic damper based on torsional yielding: part II—experimental phase, *Earthquake Engineering & Structural Dynamics*, 45(5), 2016, 779-796.
[30] Dowling, N.E., *Mechanical Behavior of Materials*, Pearson Education Limited, 2013
[31] Geem, Z.W., *Harmony search algorithms for structural design optimization*, Springer, 2009.
[32] Rothlauf, F., *Representations for Genetic and Evolutionary Algorithms*, Springer Berlin, Heidelberg, 2006.
[33] Kirkpatrick, S., Gelatt, C.D., Vecchi, M.P., Optimization by simulated annealing, *Science*, 220(4598), 1983, 671-680.
[34] Ghozi, M., Budiati, A., Comparison of Genetic Algorithm and Harmony Search Method for 2D Geometry Optimization, *MATEC Web of Conferences*, 159, 2018, 01009.
[35] Kim, Y.-H., Yoon, Y., Geem, Z.W., A comparison study of harmony search and genetic algorithm for the max-cut problem, *Swarm and Evolutionary Computation*, 44, 2019, 130-135.
[36] Peraza, C., Valdez, F., Castillo, O., *A Harmony Search Algorithm Comparison with Genetic Algorithms*, in Fuzzy Logic Augmentation of Nature-Inspired

Optimization Metaheuristics: Theory and Applications, O. Castillo and P. Melin, Editors, Springer International Publishing: Cham., 2015.
[37] Sharma, S., Pandey, H.M., Genetic Algorithm, Particle Swarm Optimization and Harmony Search: A quick comparison, *in 2016 6th International Conference - Cloud System and Big Data Engineering (Confluence)*, Noida, India, 2016.

ORCID ID

Arash Radman https://orcid.org/0000-0002-8891-2500
Saeid Pourzeynali https://orcid.org/0000-0003-2399-5621
Nima Faraji https://orcid.org/0009-0006-7105-9028

How to cite this article: Radman, A., Pourzeynali, S., Faraji, N., Optimizing multidirectional torsional hysteretic damper specifications using harmony search, *J. Appl. Comput. Mech.*, 10(1), 2024, 80–91. https://doi.org/ 10.22055/jacm.2023.43947.4148